Applied Radiation and Isotopes ▮ (▮▮▮▮) ▮▮▮–▮▮▮

Contents lists available at SciVerse ScienceDirect

Applied Radiation and Isotopes

journal homepage: www.elsevier.com/locate/apradiso

# Development of a simple detector response function generation program: The CEARDRFs code

Jiaxin Wang [a,*], Zhijian Wang [a], Johanna Peeples [a], Huawei Yu [a,b], Robin P. Gardner [a]

[a] Center for Engineering Applications of Radioisotopes (CEAR), Department of Nuclear Engineering, North Carolina State University, Raleigh, NC 27695, USA
[b] College of Geo-Resources and Information, China University of Petroleum, Qingdao, Shandong 266555, China

ARTICLE INFO

*Keywords:*
Detector response function
Scintillator
Nonlinearity
Flat continuum
CEARDRFs

ABSTRACT

A simple Monte Carlo program named CEARDRFs has been developed to generate very accurate detector response functions (DRFs) for scintillation detectors. It utilizes relatively rigorous gamma-ray transport with simple electron transport, and accounts for two phenomena that have rarely been treated: scintillator non-linearity and the variable flat continuum part of the DRF. It has been proven that these physics and treatments work well for $3\times3''$ and $6\times6''$ cylindrical NaI detector in CEAR's previous work. Now this approach has been expanded to cover more scintillation detectors with various common shapes and sizes. Benchmark experiments of $2\times2''$ cylindrical BGO detector and $2\times4\times16''$ rectangular NaI detector have been carried out at CEAR with various radiactive sources. The simulation results of CEARDRFs have also been compared with MCNP5 calculations. The benchmark and comparison show that CEARDRFs can generate very accurate DRFs (more accurate than MCNP5) at a very fast speed (hundred times faster than MCNP5). The use of this program can significantly increase the accuracy of applications relying on detector spectroscopy like prompt gamma-ray neutron activation analysis, X-ray fluorescence analysis, oil well logging and homeland security.



## 1. Introduction

Detector response function (DRF) is a very important inherent detector property, denoted by $D(E',E)$, where $E$ is incident gamma or X-ray energy and $E'$ is pulse height gamma or X-ray energy, giving the pulse height spectral energy distribution for any specific gamma-ray or X-ray incident energy. As a probability density function (pdf), the integral of DRF over all pulse height energy is unity.

Accurate detector response functions have become increasingly useful and needed for many applications, including the construction of spectral libraries for use in the Monte Carlo library least squares (MCLLS) analysis method for inverse elemental analysis of prompt gamma-ray neutron activation analysis (PGNAA) (Shyu et al., 1993; Han et al., 2007) and energy-dispersive X-ray fluorescence (EDXRF) analyzers (Li et al., 2007).

There are several advantages (Gardner and Sood, 2004) of using DRFs in Monte Carlo simulation, including (1) DRF could be pre-calculated or pre-measured and takes care of the inside tracking of detector. Thus, each gamma-ray history is tracked only outside of the detector, saving as much as 50% of total tracking time for each gamma-ray history in Monte Carlo simulation; (2) DRF can be made considerably more accurate by empirical or semi-empirical methods, which make the use of DRF yield better accuracy in spectral simulations and is critical in following least square analysis; (3) DRF could 'naturally' apply detector resolution to simulated flux spectra to smooth it. Most Monte Carlo codes including the most popular general purpose MCNP5 try to apply it directly to each history. Using DRF could further reduce the required history number by 1 or 2 magnitudes to reach the same statistical requirements.

## 2. Detector response function generation methods

Because the same detector has been repeatedly used under different situations, the particle-transport inside the detector (DRF) could be pre-generated to improve future simulation speed and accuracy. Generation of DRF usually has three ways (Gardner et al., 1986). (1) Experimental approach (Heath, 1964, 1974) is the pioneer in this area. However, there are always features that present in experimental spectrum that are not part of DRF. For example, gamma-rays that backscattered to detector from surrounding materials and 0.511 MeV annihilation photons are not legit parts of DRF. (2) Monte Carlo approach. DRF is simulated strictly following the basic principles with Monte Carlo methods, utilizing the normal exact geometrical description of detector and

* Corresponding author.
*E-mail address:* jwang3@ncsu.edu (J. Wang).

0969-8043/$ - see front matter © 2011 Elsevier Ltd. All rights reserved.
doi:10.1016/j.apradiso.2011.11.003

the exact physics of photon and electron transport. Most general purpose Monte Carlo simulation codes like MCNP5 (X-5 Monte Carlo Team, 2008) could be considered in this category. The simulation results are usually considered to be accurate enough. However, the approach is very time consuming as there are lots of interactions/scattering following full physics, while the eventual fates of lot of tracking results are to deposit all energy in the detector. Also, some features of detector are nearly impossible to determine like the imperfections within the crystal. (3) Hybrid approach. It is naturally to combine the Monte Carlo approach with some empirical or semi-empirical parameters that acquired from experiments. In this way, some unnecessary tracking of particles could be avoid to accelerate the simulation and empirical or semi-empirical parameters could be used to correct some features of detector.

## 3. Previous works at CEAR

The Center for Engineering Application of Radioisotopes (CEAR) has over 20 years' history of research on DRF. A variety of specific DRF generation models and codes were developed at CEAR in the past for both semi-conductor and scintillation detectors with the hybrid approach. For example, the semi-empirical approach for the DRF of the semiconductor Ge (Jin et al., 1986; Lee et al., 1987) and Si(Li) detectors (Yacout et al., 1986; He et al., 1990) and NaI detector (Gardner and Sood, 2004; Peplow et al., 1994). Most of these codes can generate the DRF by separate components and then sum them up. Some of the first work in generating the entire spectra was done by Berger et al. (1972). Code MONTE (Peplow et al., 1994) is the first one that demonstrated for generating entire spectra DRF for gamma rays incident on NaI detectors with improved physics. The approach was demonstrated for gamma-rays with energy from 0.5 to 10.5 MeV incidents on $3'' \times 3''$ and $6'' \times 6''$ cylindrical detectors, while source position is fixed at 10 cm away from the one surface. To properly treat the non-linearity effect of NaI crystal and the lower estimation of flat continuum, codes G03 and G04 (Gardner and Sood, 2004) were developed. At CEAR, we also maintain a local version of MCNP5 (Wang et al., 2008), which has been implanted some empirical parameters to improve accuracy and been simplified in electron transport to save simulation time.

The interest naturally expands to other scintillation detector and other detector shape and sizes (Gardner, 2005). The code CEARDRFS has been developed to generate DRFs for gamma-rays incident on scintillation detectors (NaI, BGO, etc.) with various shapes (cylinder or rectangle) and different sizes. Theoretically, it can be applied to all kinds of scintillation detectors with proper experimental data. CEARDRFS also has a very fast simulation speed. The approach used CEARDRFS is the hybrid one. Although this approach does not give much insight into the physical processes that take place inside the detector, the results show a very good accuracy.

## 4. Physics in CEARDRFS

The Monte Carlo model used in CEARDRFS to generate the entire pulse height spectra including two parts: photon treatment and electron treatment. CEARDRFS inherits a NJOY (MacFarlane) pre-processing nuclear data from other CEAR codes. The photon cross sections are extracted from EPDL library that covers all the elements from $Z=1$–100 and the energy range now from 10 KeV to 20 MeV, which make the code expandable to all kinds of scintillation detectors theoretically.

### 4.1. Photon treatment

CEARDRFs, considers only the three basic gamma-ray interactions with matter (Knoll, 2000), photoelectron effect, Compton scattering and pair production. The coherent scattering is not considered.

#### 4.1.1. Photoelectron effect

In the photoelectron absorption process, a photon undergoes an interaction with an absorber atom in which the photon completely disappears. In its place, an energetic photoelectron is ejected by the atom from one of its bound shells. The photoelectrons in this interaction are assumed to be emitted in an isotropic distribution, and binding energy is assumed to be neglectable comparing to incident gamma energy. CEARDRFs continues to track the ejected electron with electron treatments that will be described below.

#### 4.1.2. Compton scattering

The interaction process of Compton scattering takes place between the incident photon and the electron in the absorbing material. The scattered photon energy can be calculated by

$$E' = \frac{E}{1+(E/m_0c^2(1-\cos\theta)}$$

where $m_0c^2$ is the rest-mass energy of electron (0.511 MeV) and $\theta$ is the angle between the direction of scattered photon with respect to its original direction.

The angular distribution of scattered gamma rays is predicted by Klein – Nishina formula for the differential cross section $d\sigma/d\Omega$:

$$\frac{d\sigma}{d\Omega} = Zr_0^2\left(\frac{1}{1+\alpha(1-\cos\theta)}\right)^2\left(\frac{1+\cos^2\theta}{2}\right)\left(1+\frac{\alpha^2(1-\cos\theta)^2}{(1+\cos^2\theta)[1+\alpha(1-\cos\theta)]}\right)$$

where $\alpha = h\nu/m_0c^2$ and $r_0$ is the classical electron radius. Kahn rejection method (Kahn, 1994) is used in CEARDRFS to sample the angle $\theta$. The scattered gamma-rays continue to be tracked until meeting the terminating conditions.

The incident photon transfers a portion of its energy to the recoil electron. The recoil electron energy $E_{e-}$ and the direction $\theta_e$ of recoil electron with respect to the original photon direction can be calculated by the following equation, and continues to be tracked with electron treatments:

$$E_{e-} = E - E' \quad \cos\theta_e = \frac{E/E' - \cos\theta}{\sqrt{(E/E')^2 - 2(E/E') + 1}}$$

#### 4.1.3. Pair production

If the gamma-ray energy exceeds twice the rest-mass energy of an electron (1.02 MeV), the process of pair production is energetically possible. In the interaction that must take place in the Coulomb field of a nucleus, the incident photon disappears and is replaced by an electron – positron pair. All the excess energy carried in by the photon above 1.02 MeV required to create the pair goes into kinetic energy share by the positron and electron. The available energy for the electron ($E_{ekin}$) and positron ($E_{pkin}$) is evenly split between them:

$$E_{pkin} = E_{ekin} = \tfrac{1}{2}(E - 2m_0c^2)$$

The polar angle, $\theta_p$, of the emission for the electron and positron is assumed to be selected randomly between 0 and $\theta_m$ (Shultis and Richard, 2000):

$$\cos\theta_m = m_0c^2/E$$

Then the azimuthal angle $\theta_z$ is chosen isotropically and the positron azimuthal angle is taken as the opposite ($\theta_z \pm 180^\circ$). Both

Please cite this article as: Wang, J., et al., Development of a simple detector response function generation program: The CEARDRFs code. Appl. Radiat. Isotopes (2011), doi:10.1016/j.apradiso.2011.11.003

the electron and position will continue to be tracked in CEARDRFS with the simple electron treatments.

If the positron will eventually annihilate after slowing down in the detector, two annihilation photons are produced. Each of them has an energy equivalent to the rest mass of the electron. The direction of the first photon is chosen isotropically and the second is taken to be in exactly the opposite direction. The subsequent fat of this annihilation radiation has an important effect on the response of gamma-ray detectors. The two annihilation photons then track separately until they meet the termination conditions.

There are three ways to terminate gamma particle history: (1) gamma particle escape the system; (2) gamma particle has photoelectric interaction and (3) gamma particles energy is lower than the energy cut.

### 4.2. Electron treatment

An electron is slowed down as a result of both Columbic interactions with (atomic) electrons and radiation loss (Bremsstrahlung). Range, the continuous slowing-down approximation combining with Bremsstrahlung, is usually a good approximation for electron transport.

### 4.3. Electron range

The first step of the treatment for electron transport is calculating the range of the electron, $R_e$, through the medium without any major interactions. The equation (Katz and Penfold, 1952) used to calculate range $R_e$ is

$$R_e = \frac{aE^{(b-c\ln E)}}{\rho}$$

where $R$ is in cm, $E$ is in MeV, $\rho$ is in g/cm$^3$, and $a$, $b$, $c$ are empirical parameters. All $a$, $b$ and $c$ values (Table 1) are fitted with Pages' data (Pages et al., 1972) for NaI detector and BGO detector. For BGO, the weighted summation of bismuth, germanium and oxygen was used. Then the densities of NaI and BGO are 0.3667 g/cm$^3$ and 7.13 g/cm$^3$, respectively.

According to electron range, the distance traveled without interaction by an electron with certain energy needs to be sampled. An electron continues in a straight line losing energy by ionization continuously until a major interaction occurs and takes it out of the original path direction. Then, the probability distribution function for the distance traveled $d$ by the electron before a major interaction occurs would be uniform between zero and the calculated range $R_e$. If not leaving the detector, the electron will be updated to a new position.

The electron loses energy by ionization as it moves through this distance. Using this range−energy relationship, the new energy of electron, $E'$, after moving through distance $d$ and losing energy due to ionization collisions is calculated to be

$$E' = \exp\left[\frac{b}{2c} - \sqrt{\left(\frac{b}{2c}\right)^2 - \frac{1}{c}\ln\left(\frac{\rho(R_e-d)}{a}\right)}\right]$$

**Table 1**
Range parameters for NaI and BGO detector calculated from Pages' data.

| | $a$ | $b$ | $c$ |
|---|---|---|---|
| NaI | 0.69361 | 1.15080 | 0.083893 |
| BGO($E<=0.1$ MeV) | 0.68223 | 1.24847 | 0.068837 |
| BGO(0.1 MeV$<E<=1$ MeV) | 0.69894 | 1.14744 | 0.119043 |
| BGO($E>1$ MeV) | 0.70506 | 1.10863 | 0.080150 |

The difference between the original energy of the electron and its new energy is deposited in the detector, as long as the path does not leave the detector.

#### 4.3.1. Bremsstrahlung radiation

After traveling to major interaction at a new position inside the detector, the direction of the electron will change. The radiation energy loss of the electron by production of bremsstrahlung radiation contributes to the change. Radiative energy loss is dominant for electrons at higher energy while ionization energy loss is dominant for lower energy and is characterized by the stopping power. Instead of modeling the radiative production of bremsstrahlung by use of the stopping power, empirical value $\tau$ was used as an approximation, which means for an electron kinetic energy, $T$, the ratio, $\tau$, of the major interactions that are treated as producing bremsstrahlung radiation:

$$\tau = \begin{cases} eff \cdot T & T \le 10/eff \text{ MeV} \\ 1 & T > 10/eff \text{ MeV} \end{cases}$$

The *eff* values in Table 2 were found empirically to make the spectra similar to experiments.

It is easy to understand that for the same scintillator, the larger the size, the less possible that bremsstrahlung photon will eventually escape. For BGO detector, because it is denser than NaI, there are less bremsstrahlung photons escaping from detector than the same size NaI detector. For the rectangular NaI detector, the large surface is usually used in detection, which raises the possibility that bremsstrahlung photons escape from detector.

The energy of bremsstrahlung photons is picked from a distribution given by Hansen and Fultz (1960). An energy scaled version of this curve is used for other energies. The electron angle is scattered at 90° and the photon is emitted in the original direction of the electron. The electron continues with an energy reduced by the energy of bremsstrahlung photon. Both electron and photon are tracked until meeting the termination conditions.

#### 4.3.2. Terminating the electron

There are also two ways to terminate electron history: (1) electron escapes the system and (2) electron energy is lower than the cut-off.

## 5. Adjustments in CEARDRFs

Following the above physics, it is still not good enough to produce accurate DRF. Certain adjustments need to be done in CEARDRFS including scintillators nonlinearity and flat continuum adjustment. Also, to account for detector resolution, proper Gaussian broadening parameters need to be extracted from experiments.

### 5.1. Nonlinearity

Nonlinearity effect in scintillation detectors is of great interests nowadays as it affects the peak positions, especially the escape peaks (Gardner and Sood, 2004). Although there is no widely accepted explanation about this phenomenal, Rooney and

**Table 2**
Empirical *eff* parameter for NaI and BGO detector.

| | $3''\times3''$ NaI [a] | $6''\times6''$ NaI [a] | $2''\times2''$ NaI | $2''\times2''$ BGO | $2''\times4''\times16''$ NaI |
|---|---|---|---|---|---|
| *Eff* | 0.3 | 0.2 | 0.5 | 0.25 | 0.25 |

[a] Berger and Seltzer (1972) and Halbleib et al. (1992).

Please cite this article as: Wang, J., et al., Development of a simple detector response function generation program: The CEARDRFs code. Appl. Radiat. Isotopes (2011), doi:10.1016/j.apradiso.2011.11.003

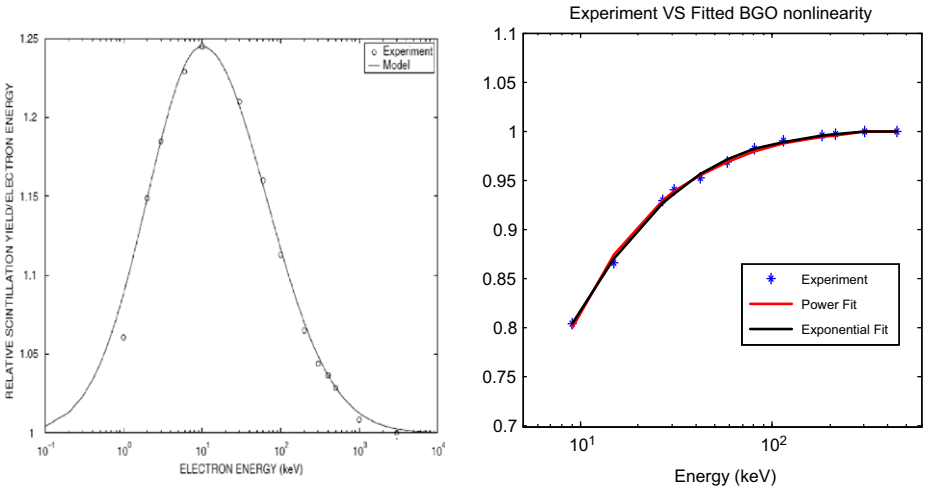


**Fig. 1.** Experiment versus model for NaI (left) and BGO (right) nonlinearity with electron energy.

Valentine (1996, 1997), Valentine and Rooney (1994) and Valentine et al. (1998a, 1998b) have done good experiments to quantify this phenomena in different kinds of scintillation detectors by a Compton coincidence technique (CCT). They treat the scintillation detectors nonlinearity with electron energy deposited. The electron energy versus relative scintillation yield per electron energy for NaI and BGO could be plotted in Fig. 1 as follows based on Rooney and Valentine's work, and then empirical models were fitted to describe this relationship.

The following relationship can be used to formulate the relative NaI and BGO scintillation efficiency versus deposited electron energy (light yield per electron energy):

$$N_e(E_e) = a + b\exp\left(\frac{-(\ln E_e - k_1)^{k_2}}{k_3}\right)$$

The model data versus experiments are also plotted in Fig. 1, and the five parameter values are listed in Table 3. The equation has been put in CEARDRFS code to handle scintillation detector nonlinearity. When an electron deposits all or part of its energy in the detector, the tallied energy $E_t$ will be the energy deposited multiplied by scintillation efficiency $N_e$:

$$E_t = N_e(E_{edep})E_{edep}$$

The simulated flux spectra (without considering detector resolution) for Na-24 high energy peak (2.754 MeV) with linear scintillation efficiency, NaI and BGO nonlinearity are plotted in Fig. 2. The three peaks are full energy peak, single escape peak and double escape peak from high energy to low. It is easy to see that NaI nonlinearity has a large influence on the peak positions (shift to right side) and has different effects on different energy peaks (single escape peak is shifted further to the right than other two). BGO nonlinearity's influence is small, a little bit shift to lower energy side. The difference between incident gamma energy and pulse height gamma energy (peak position on flux spectra) is the result of scintillator nonlinearity. After putting in the nonlinearity, the detector response function could match the experimental spectra very well as shown previous work (Gardner and Sood, 2004).

Normally, this nonlinearity depends only on scintillators type. When we tried to apply this to rectangular shape NaI detector ($2'' \times 4'' \times 16''$), which is commonly used in homeland security application, we found that it is not as nonlinear as the cylinder shape. The largest face was used in experiment. Thus, light transport efficiency parameter *lte* was introduced to account for the light loss in transport, which is quite normal in long shape detector. For the detector we tested, $lte = 0.2$ will make the simulated detector response function match experiments well.

**Table 3**
Empirical parameters for NaI and BGO detector nonlinearity.

| | $a$ | $b$ | $k_1$ | $k_2$ | $k_3$ |
|---|---|---|---|---|---|
| NaI ($E_e \le 10$ keV) | 1.000 | 0.245 | 2.3026 | 2 | 5.1946 |
| NaI ($E_e > 10$ keV) | 1.000 | 0.245 | 2.3026 | 2 | 7.1635 |
| BGO | 1.0006 | −0.3862 | 0.4918 | 1.8224 | 3.9363 |

### 5.2. Flat continuum

With basic principles that utilize the normal exact geometrical description of the detector and the exact physics of photon and electron transport, the intensity of Compton continuum in Monte Carlo generated DRF is often as much as an order of magnitude or more smaller than observed in experiments (Gardner and Sood, 2004). The physical mechanism of this phenomenon is not very clear, but it is believed that detector imperfections and electron channeling from the detector crystal are the reasons. Both detector imperfection and electron channeling are not easy to put in the Monte Carlo simulation if not unknown. Thus, a pseudo-electron range by a trial-and-error fit to experimental results to take care of the unknown extent of these detector phenomena. In practice, the electron range in CEARDRFS is multiplied by an arbitrary value. The best multiplier will be determined by trial-and-error for the detector case of interest.

In pevious's work (Gardner and Sood, 2004), a model form for the electron range multiplier is taken as

$$R_e = 1 + A_1\exp(-A_2E_I) + A_3\exp(-A_4E_I)$$

$$A_1 = 39.662, A_2 = 3.4052, A_3 = 1.5434, A_4 = 0.1576$$

where $E_I$ is the incident photon energy, $A_1 - A_4$ are parameters to be derived from experimental data. This model approaches unity as incident photon energy is going higher. However, the author found that this model cannot be expanded to BGO detector and NaI detector in other shapes. Although proper multiplier could be determined through trial-and-error to fit the experiments well, more experimental data are still needed to derive reliable models for these detectors.

Please cite this article as: Wang, J., et al., Development of a simple detector response function generation program: The CEARDRFs code. Appl. Radiat. Isotopes (2011), doi:10.1016/j.apradiso.2011.11.003

### 5.3. Gaussian broadening

Due to the finite resolution of real radiation detectors and statistical effects, the measured spectrum for a mono-energetic photon source will appear as a broadened peak at the source energy. The shape of this peak is approximately Gaussian distribution as follows with the center at the source energy and a width that is characteristic of the specific detector:

$$G(E)=\frac{A}{\sigma\sqrt{2\pi}}\exp\left(-\frac{(E-E_0)^2}{2\sigma^2}\right)$$

where $E$ is the broadened energy, $E_0$ is the energy of the tally, $A$ is normalization constant and $\sigma$ is the Gaussian standard deviation.

The initial tallied spectrum from CEARDRFS is not a "real" spectrum, it is a kind of "spectra flux" without considering the effect of detector resolution as shown in Fig. 2. Thus, proper Gaussian broadening should be applied to the "spectra flux" to get a practical DRF. To determine the Gaussian distribution, people need to know the mean, which is incident particle energy and standard deviation. The formula used in MCNP5 (X-5 Monte Carlo Team, 2008) to calculate $\sigma$ is specified as follows:

$$\sigma=FWHM/\sqrt{8\ln 2}=FWHM/2.3548\quad FWHM=a+\sqrt{b(E+cE^2)}$$

where $E$ is the photon particle energy in MeV and $a$, $b$ and $c$ are user-provided Gaussian parameters, FWHM is the full width half maximum, which could be determined from experiments. Instead of using the same formula as MCNP5, we found that the following formula is also a good choice:

$$\sigma=dE^e$$

where $\sigma$ is the standard deviation in MeV and $E$ is the photon particle energy in MeV. Only two parameters are needed and after taking the natural logarithm on both sides, the two parameters could be determined from linear equation:

$$\ln\sigma=\ln d+e\ln E$$

For example, Table 4 could be obtained from experiments of $2''\times 2''$ NaI detector experiments, and the linear fitting of above formula is shown in Fig. 3. The experimentally determined Gaussian broadening parameters are listed in Table 5 for various detectors. Although there is a slight difference between different detectors, even in the same size, the table can serve as a reference and is the default data in CEARDRFS. One issue should be pointed

**Table 4**
Experimental data of $2''\times 2''$ NaI detector to determine Gaussian broadening parameters.

| $E$ (MeV) | $E_{low}$ | $E_{high}$ | FWHM | Sigma | ln $E$ | ln $\sigma$ |
|---|---|---|---|---|---|---|
| 0.411(Au198) | 0.3912 | 0.4309 | 0.0397 | 0.016859 | −0.88916 | −4.08287 |
| 0.662(Cs137) | 0.6357 | 0.6857 | 0.05 | 0.021233 | −0.41249 | −3.8522 |
| 1.12(Sr46) | 1.0832 | 1.1558 | 0.0726 | 0.03083 | 0.113329 | −3.47925 |
| 1.332(Co60) | 1.2883 | 1.3701 | 0.0818 | 0.034737 | 0.286682 | −3.35994 |
| 2.754(Na24) | 2.6777 | 2.8244 | 0.1467 | 0.062298 | 1.013054 | −2.77583 |

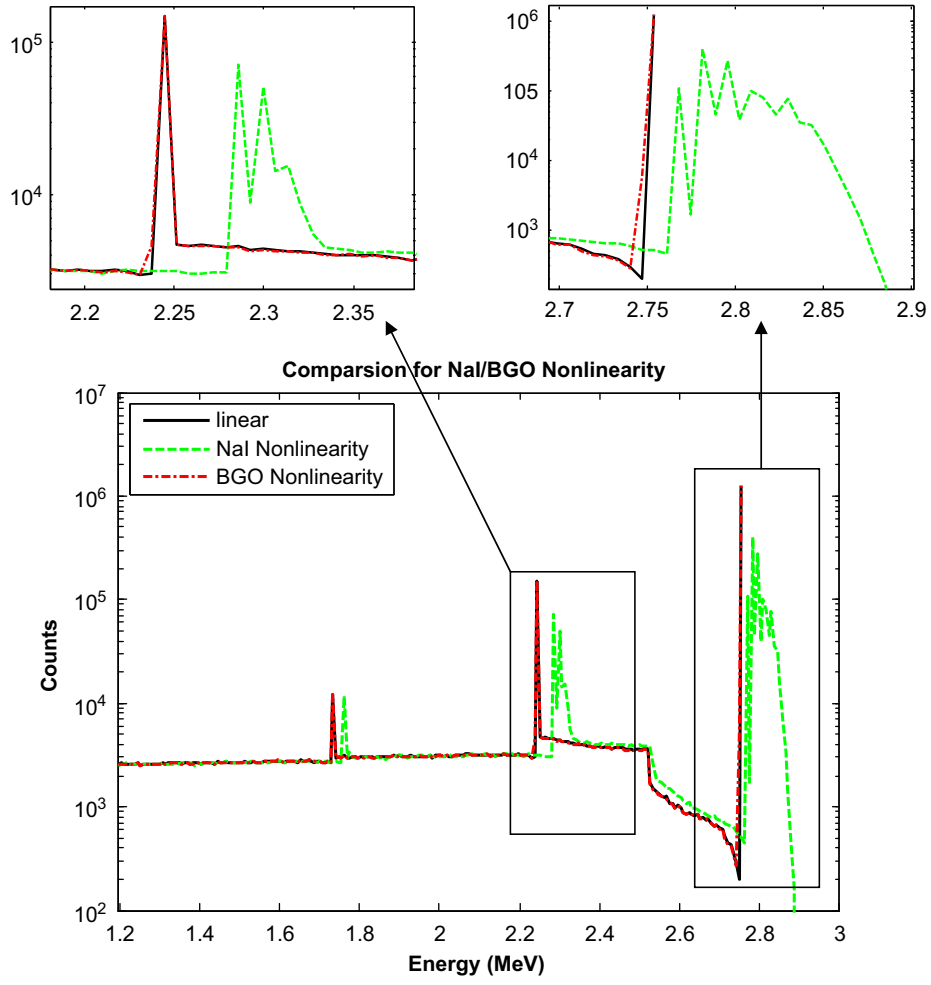


**Fig. 2.** Simulated nonlinearity effect of NaI and BGO detector for 2.754 MeV photon.

out is the additional broadening introduced by nonlinearity, which should be compensated. More details could be found in Gardner's research (Gardner and Sood, 2004).

In CEARDRFS, Gaussian broadening is applied after all simulation histories have been done instead of applying to each history as MCNP5 does. Some researchers (Metwally et al., 2004; Gardner et al., 2007) show that this approach can reduce the total number of histories of the simulation by up to two orders of magnitude to reach the same statistical requirements.

## 6. Benchmark experiments

Cylindrical NaI DRFs generated by G03, the former version of CEARDRFS, have been proven to agree with experiments well and show a large improvement over MCNP5 generated DRFs (Gardner and Sood, 2004). After expanding to new scintillators and more shapes, more benchmark experiments have been done.

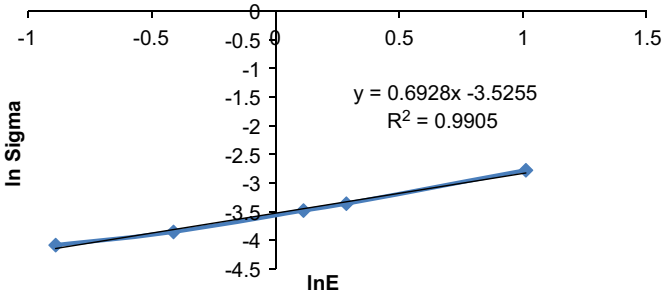


**Fig. 3.** Linear fitting of Gaussian broadening parameters on $2'' \times 2''$ NaI experimental data.

**Table 5**
Gaussian broadening parameters for different detectors.

| | $2'' \times 2''$ NaI | $3'' \times 3''$ NaI | $6'' \times 6''$ NaI | $2'' \times 2''$ BGO | $2'' \times 4'' \times 16''$ NaI |
|---|---|---|---|---|---|
| d | 0.02953 | 0.03027 | 0.02609 | 0.04221 | 0.02721 |
| e | 0.6928 | 0.6593 | 0.6027 | 0.6363 | 0.6224 |

### 6.1. Experiments setup

The experiment setup shown in Fig. 4 (left) was used by Heath. The source is 10 cm away from the center of front face of detector. The detector is shielded in a thick lead box. The major difference between the conditions of the heath experiments and the CEARDRFs conditions are (1) the experiments were done in air rather than

**Table 6**
Radioisotopes used in CEAR experiments.

| | Cs-137 | | Co60 | | Na24 | | Al28 |
|---|---|---|---|---|---|---|---|
| Energy (MeV) | 0.662 | 0.033[a] | 1.173 | 1.332 | 1.368 | 2.754 | 1.779 |
| Probability | 0.8998 | 0.0727 | 1.00 | 1.00 | 0.9999 | 0.9986 | 1.00 |

[a] Combination effects from particles Ba137 m.

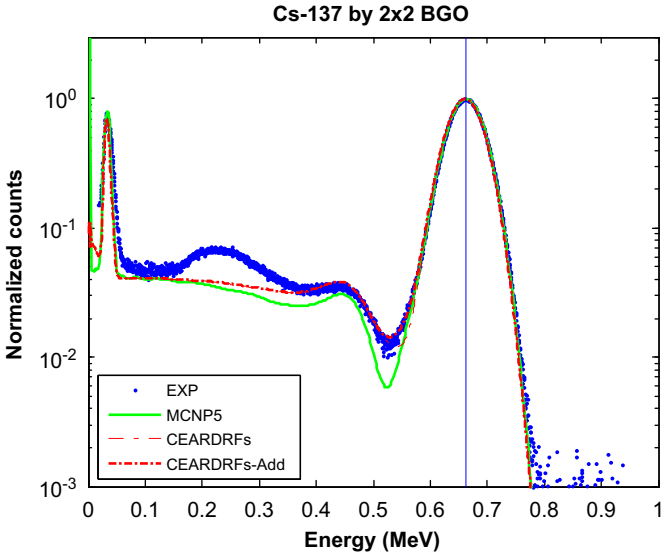


**Fig. 5.** Comparison among Cs137 experiment, MCNP DRF and CEARDRFs DRF for $2'' \times 2''$ BGO.

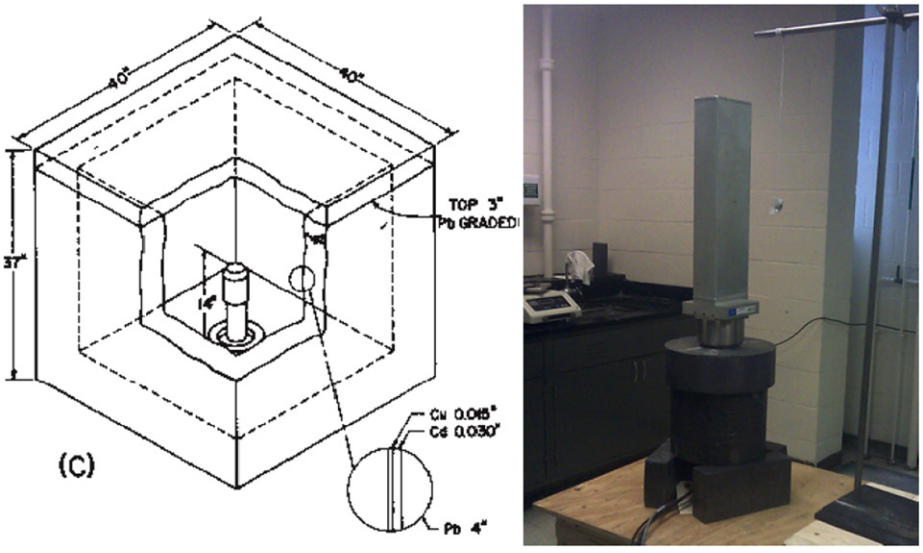


**Fig. 4.** Experiment setup of Heath (left) and rectangular NaI detector at CEAR (right).

Please cite this article as: Wang, J., et al., Development of a simple detector response function generation program: The CEARDRFs code. Appl. Radiat. Isotopes (2011), doi:10.1016/j.apradiso.2011.11.003

vacuum; (2) the experiments have surroundings, like lead shielding, rather than being in an infinite vacuum, and there are aluminum can around the detector and PMT; (3) the CEARDRFs only treats a single gamma-ray energy and does not consider beta particles or other gamma-rays that might be present from a given radioisotopes.

Thus, our experiments were carried out in a big empty room to reduce the scattering from the surrounding environments, although the scattering cannot be eliminated thoroughly. For cylindrical detectors, the radioisotopes were placed 10 cm away from the center of surface. For rectangular detector, they were placed 10 cm away from the center of the largest surface.

In the following comparisons, if more than one gamma-ray energy is emitted from radioisotopes, then CEARDRFS generated single energy DRF will be summed up according to the emitting percentage to compare to experiments. Four radioisotopes were used to verify CEARDRFS generated DRF (Table 6).

### 6.2. $2'' \times 2''$ BGO cylindrical detector

The comparisons among experiments, MCNP5 generated DRFs and CEARDRFS generated DRFs for $2'' \times 2''$ BGO cylindrical detector are plotted in Figs. 6–8. All spectra are normalized to their highest peaks. Overall, CEARDRFS generated DRFs show large improvements over MCNP5 generated DRFs and agree with CEAR experiments well. The improvements include more accurate full energy peak to Compton continuum ratio, full energy peak to full energy peak ratio and full energy peak to escape peaks ratio, better valley shape, and more accurate peak positions after proper gain-shifting.

Please note that, in Figs. 5 and 6, the peaks around 0.2–0.3 MeV are backscattering peaks, which originate from the gamma-rays that scattered back from surrounding materials. The backscattering peak is not a legit part of DRF as stated in previous section. For Na24 and Al28, we had to make them from PULSTAR

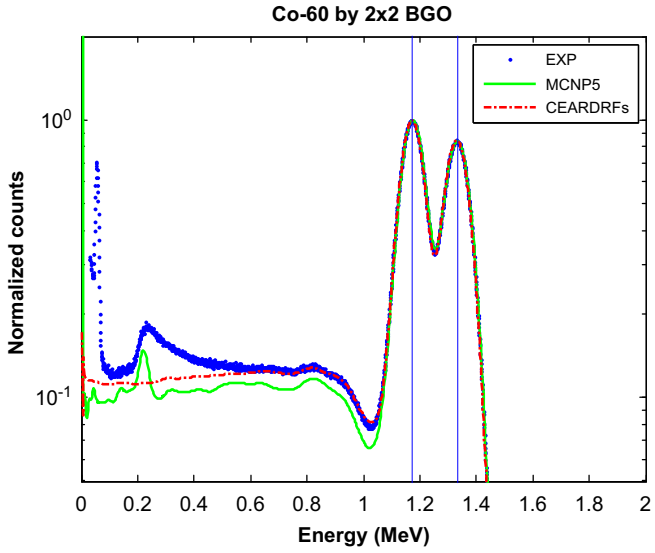


**Fig. 6.** Comparison among Co60 experiment, MCNP DRF and CEARDRFs DRF for $2'' \times 2''$ BGO.

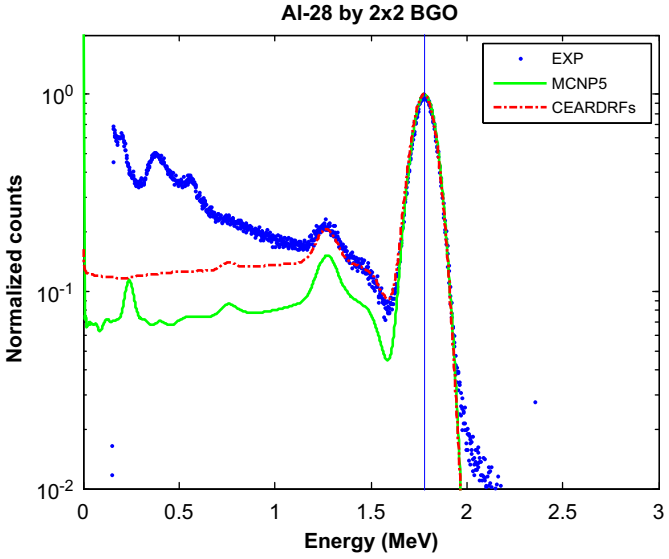


**Fig. 8.** Comparison among Al28 experiment, MCNP DRF and CEARDRFs DRF for $2'' \times 2''$ BGO.

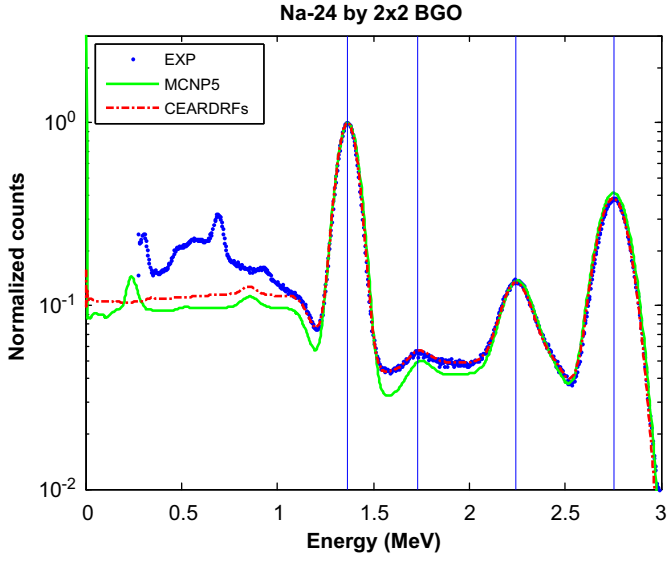


**Fig. 7.** Comparison among Na24 experiment, MCNP DRF and CEARDRFs DRF for $2'' \times 2''$ BGO.

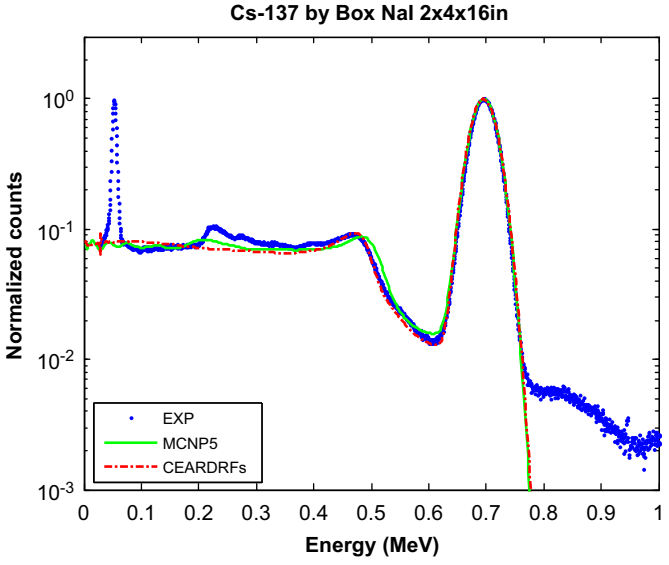


**Fig. 9.** Comparison among Cs137 experiment, MCNP DRF and CEARDRFs DRF for $2'' \times 4'' \times 16''$ NaI.

Please cite this article as: Wang, J., et al., Development of a simple detector response function generation program: The CEARDRFs code. Appl. Radiat. Isotopes (2011), doi:10.1016/j.apradiso.2011.11.003

reactor at NCSU as they are short life isotopes. For some reasons, there were some contaminations, which contribute to the low energy parts in Figs. 7 and 8. In Fig. 6, the difference between spectra CEARDRFs and CEARDRFs-add is the X-ray escape peak from BGO crystal was added back in the second spectra, which makes a perfect shape of the low energy side of full energy peak. As energy goes higher, this has not to be treated separately.

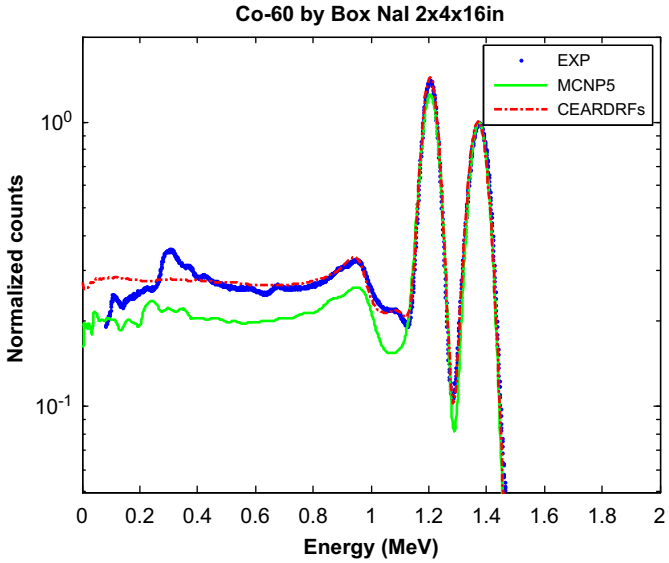


**Fig. 10.** Comparison among Co60 experiment, MCNP DRF and CEARDRFs DRF for $2'' \times 4'' \times 16''$ NaI.

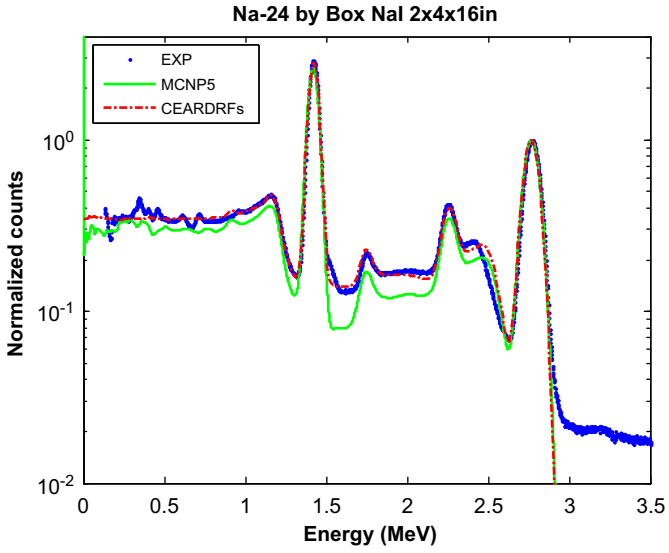


**Fig. 11.** Comparison among Na24 experiment, MCNP DRF and CEARDRFs DRF for $2'' \times 4'' \times 16''$ NaI.

### 6.3. $2'' \times 4'' \times 16''$ NaI rectangle detector

The comparisons among experiments, MCNP5 generated DRFs and CEARDRFS generated DRFs for $2'' \times 4'' \times 16''$ BGO cylindrical detector are plotted in Figs. 9–11. All spectra are normalized to their highest peaks. Overall, CEARDRFS generated DRFs show large improvements over MCNP5 generated DRFs and agree with CEAR experiments quite well. Other discussions are similar to $2'' \times 2''$ BGO detector.

## 7. Conclusions and applications of CEARDRFS

The code CEARDRFS can generate very accurate detector response function for cylindrical or rectangular NaI and BGO detectors as shown in previous sections. With empirical implements of scintillation detector nonlinearity, flat continuum adjustment and Gaussian broadening, there are big improvements over the most popular and widely recognized general purpose Monte Carlo code MCNP5. Also, the generation of detector response function is much faster than MCNP5. For 2.754 MeV energy, only 59 s are needed for the execution of CEARDRFS. That is over hundreds of times speed improvements that benefited from the hybrid empirical approaches. Also, with user provided parameters, the code CEARDRFS can be easily expanded to other type of scintillators such LaBr, LSO, etc. We currently do not hold these types of detectors at CEAR. Otherwise, these empirical parameters will have been put in the code.

The flow chart of the whole process is plotted in Fig. 12. As it shows, the code CEARDRFS is usually used with another Monte Carlo code to handle the outside of detector. It could be some specified purpose code like CEARXRF or CEARCPG that we have been using, or other general purpose Monte Carlo code like MCNP5. For better accuracy, the path length through detector of the incident gamma-rays should be recorded to adjust the weight when scoring, as the source position fixed in CEARDRFS when generating detector response function.

PGNAA is a good example to show the application of DRF. In the PGNAA application, the specified purpose Monte Carlo code is used to simulate particles outside the detector and first tracking the prompt gamma rays to the point that they are incident on the detector. These incident gamma-ray spectra or called flux spectra for each element are saved and DRF is subsequently used to convolute these spectra into detected pulsed-height spectra. Then further spectra analysis, like library least square, could be applied with the simulated pulsed-height spectra and the experimental spectra. Therefore, accurate detector response functions are very critical to the PGNAA application.

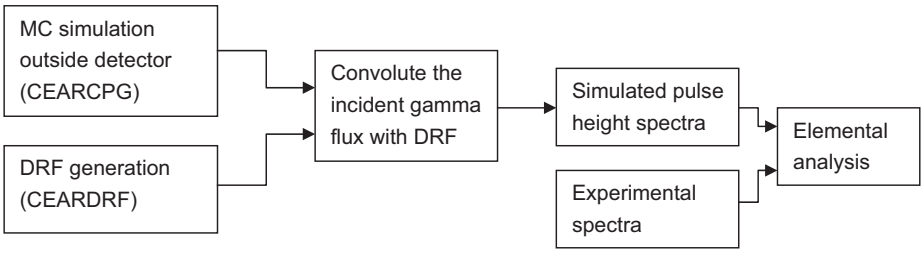


**Fig. 12.** General flow chart of PGNAA application with DRF.

Please cite this article as: Wang, J., et al., Development of a simple detector response function generation program: The CEARDRFs code. Appl. Radiat. Isotopes (2011), doi:10.1016/j.apradiso.2011.11.003

## Acknowledgments

The authors gratefully acknowledge the support of the CEAR Associates Program on Nuclear Techniques in Oil Well Logging that includes Baker Atlas, Halliburton, Weatherford, EXXON Mobil, Pathfinder, and Los Alamos National Laboratory. The authors also appreciate our Reactor Health Physicist, Mr. Gerald Wicks, to help make radioisotopes with PULSTAR nuclear reactor.

## References

Berger, M.J., Seltzer, S.M., 1972. Nuclear Instruments and Methods 104, 317–322.
Gardner, R.P., Sood, A., 2004. Nuclear Instruments and Methods B, 87–99.
Gardner, R.P., Yacout, A.M., Zhang, J., Verghese, K., 1986. Nuclear Instruments and Methods in Physics Research A242, 399–405.
Gardner, R.P., 2005. Transactions of the American Nuclear Society 93, 423–424.
Gardner, R.P, Xu, L., Wang, J., 2007. SPWLA 48th Annual Logging Symposium, June 4–7.
Han, X., Gardner, R.P., Metwally, W.A., 2007. Nuclear Science and Engineering 155 (1), 143–153.
Heath, R.L., 1964. Scintillation Spectrometry, Gamma-ray Spectrum Catalogue, vol. 2, 2nd ed., USAEC Report IDO-16880.
Heath, R.L., 1974. Gamma-ray Spectrum Catalogue, Ge (Li) Spectrometry, USAEC Report ANC-1000.
He, T., Gardner, R.P., Verghese, K., 1990. Nuclear Instruments and Methods in Physics Research A299, 354–366.
Halbleib, J.A., Kensek, R.P., Mehlhorn, T.A., Valdez, G., Seltzer, S.M. and Berger, M.J., 1992. Report SAND91-1634, Sandia Nat. Labs.
Hansen, N.E., Fultz, S.C., 1960. Report UCRL6099.
Jin, Y., Gardner, R.P., Verghese, K., 1986. Nuclear Instruments and Methods in Physics Research A242, 416–426.
Knoll, G.F., 2000. Radiation detection and measurement. Wiley, New York.
Kahn, H., 1994. Application of Monte Caro. USAEC Report AECU-3259. Rand Corporation.
Katz, L., Penfold, A.S., 1952. Reviews of Modern Physics 24 28.
Li, F., Guo, W., Gardner, R.P., 2007. Advances in X-Ray Analysis 51 9 pages.
Lee, M.C., Verghese, K., Gardner, R.P., 1987. Transactions of the American Nuclear Society 55, 555–557.
MacFarlane R.E., LA-12740-Rept. No.M, Los Alamos, N.M.
Metwally, W.A., Gardner, R.P., Sood, A., 2004. Transactions of the American Nuclear Society 91, 789–790.
Peplow, D.E., Gardner, R.P., Verghese, K., 1994. Sodium iodide detector response functions using simplified Monte Carlo simulation and principal components. Nuclear Geophysics 8 (3), 243–259.
Pages, L., Bertel, E., Joffre, H., Sklavenitis, L., 1972. Atomic Data and Nuclear Data Tables 4, 1–27.
Rooney, B.D., Valentine, J.D., 1996. IEEE Transactions on Nuclear Science 43 (3), 1271.
Rooney, B.D., Valentine, J.D., 1997. IEEE Transactions on Nuclear Science 43 (3), 1271.
Shyu, C.M., Gardner, R.P., Verghese, K., 1993. Nuclear Geophysics 7 (2), 241.
Shultis, J.K, Richard E. Faw, 2000. Radiation Shiledling.
Valentine, J.D., Rooney, B.D., 1994. Nuclear Instruments and Methods A 353, 37.
Valentine, J.D., Rooney, B.D., Li, J., 1998a. IEEE Transactions on Nuclear Science 45 (3), 512.
Valentine, J.D., Rooney, B.D., Dorenbos, P., 1998b. IEEE Transactions on Nuclear Science 45 (3), 1750.
Wang, Z., Speaker, D.P., Gardner, R.P., 2008. Transactions of the American Nuclear Society 98, 585–586.
X-5 Monte Carlo Team, 2008. LA-UR-03-1987, Los Alamos National Laboratory).
Yacout, A.M., Gardner, R.P., Verghese, K., 1986. Nuclear Instruments and Methods in Physics Research A243, 121–130.

Please cite this article as: Wang, J., et al., Development of a simple detector response function generation program: The CEARDRFs code. Appl. Radiat. Isotopes (2011), doi:10.1016/j.apradiso.2011.11.003